Research Report

98-15

Nonlinear Modeling and Simulation of Single Phase Doubly Salient Permanent Magnet Generator

B. Sarlioglu, T.A. Lipo

Wisconsin Power Electronic Research Center
University of Wisconsin-Madison
Madison WI 53706-1691

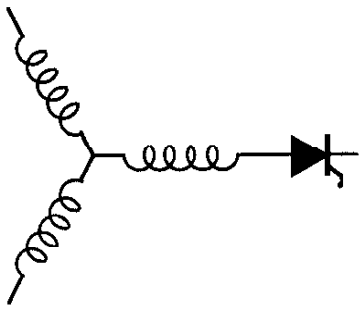

Wisconsin
Electric
Machines &
Power
Electronics
Consortium

University of Wisconsin-Madison
College of Engineering
Wisconsin Power Electronics Research Center
2559D Engineering Hall
1415 Engineering Drive
Madison WI 53706-1691

© 1998 Confidential

Nonlinear Modeling and Simulation of Single Phase Doubly Salient Permanent Magnet Generator

Bulent Sarlioglu Thomas A. Lipo
University of Wisconsin - Madison
Electrical and Computer Engineering Department
1415 Engineering Dr. Madison, WI 53706
sarliogl@cae.wisc.edu lipo@engr.wisc.edu
Fax: US + 608 262 1267

Abstract - **This paper presents the nonlinear modeling and simulation of a newly conceived doubly salient permanent magnet (DSPM) generator. Since a DSPM machine is highly nonlinear like a switched reluctance machine, utilization of generalized machine theory or lumped parameter modeling is not applicable. Utilization of first order approximations for inductance and back emf waveforms in simulations does not yield an accurate analysis. Therefore, a numerical approach using cubic splines is developed to extract useful information such as position and current dependent inductance and back emf terms from the flux linkage/current/rotor position relationship. This approach is inherently more accurate than using the first order approximations, and general enough that it can be applied to any other highly-nonlinear machines, such as a switched reluctance machine. The accuracy of the approach is also verified with experimental data.**

1. INTRODUCTION

New doubly salient permanent magnet (DSPM) ac machines, in which the field is excited by either stationary or rotating magnets, have recently been undergoing development at the University of Wisconsin-Madison [1-6]. The design of machines with a doubly salient structure with conventional approaches is not sufficiently accurate due to the many assumptions required. For example, assumptions made in conventional magnetic design for the switched reluctance machine (SRM) include neglecting or simplification of the saturation effect of the iron, fringing at the non-overlapping stator and rotor pole tips, and uneven distribution of the flux density. In the DSPM generator, there are two more nonlinearities concerned with inner and outer leakage flux of the permanent magnets. While conventional magnetic circuit design may be sufficient for an initial estimation of parameters for the DSPM machine, early designs have shown the need for refining the accuracy of the design method. However, it is more important to use these results gainfully to understand the behavior of this machine with power electronic circuitry, since the design goal is an optimized match for the performance of the machine and power electronics circuitry together, as in the case of a SRM drive.

Two major contributions beyond the originality of the generator itself have helped dramatically to demonstrate more about the nature of the DSPM machine topology. Finite element method (FEM) analyses have been carried out not only to observe the flux distribution, but also to use the results more effectively to achieve high design accuracy and dynamic modeling capability. Therefore, the first contribution has been to modify the design method and evaluate the pitfalls of the analytical design by taking into account nonlinear results obtained from FEM analysis. The second contribution is to use FEM results to obtain flux vs. current data for different rotor positions for use in a *dynamic simulation*, which is less often reported in the literature [7-11]. Since dynamic modeling for simulating the machine and power electronic circuitry together requires the partial derivative of the flux with respect to current where rotor position is a parameter, and the partial derivative of the flux with respect to rotor position where the current is a parameter, interpolation of these resulting curves is critical. It is shown in this paper that such interpolation can be achieved via cubic or B-splines. More interestingly, it is shown that simple interpolation with cubic splines may not be sufficient after the derivation process since there remain oscillatory effects due to the very high sensitivity of the numerical analysis. To prevent this oscillation, an improved interpolation method using the least squares of the error has been developed.

Various attempts have been made to model the flux linkage/current/rotor position relationship. Piecewise first- or second-order functions of flux linkage with respect to rotor position, with current as an undetermined parameter, are used for a rapid SRM computer algorithm in reference [7]. A quasi-linear model for an SRM was presented in reference [10] in which two lines are used to represent saturated and unsaturated portions of the flux linkage/current curves. In reference [11], authors solve the voltage equations by using an input table $i(\lambda,\phi)$, and intermediate values of $i(\lambda,\phi)$ required in the integration of the voltage equation are obtained by linear interpolation in rotor angle and quadratic interpolation in flux linkage instead of partial derivatives of the flux linkage.

In this paper, cubic splines are used to model the flux linkage/current/rotor position data obtained from FEM analysis. In this manner, the instantaneous inductance and back emf values can be quantified and compared with conventional design results, and therefore more insight can be gained for a better design. Finally, these results are used for a more accurate dynamic simulation of the machine and power electronics circuitry.

2. PHYSICAL CONSTRUCTION AND MODELING OF DSPM GENERATOR

The theory, modeling, and finite element analysis of the DSPM generator is given in detail in Reference [1]. However, a summary of the geometry and modeling of the DSPM generator will be given in this section to familiarize the reader with this novel generator. Fig. 1 illustrates a basic 2-phase, 4/6 pole DSPM generator. It can be noted that the stator of the DSPM generator has four poles. Two

rare earth permanent magnets are placed inside the stator yoke to provide field excitation for generator action. There is no other electrical excitation in the generator. The rotor of the basic generator has six poles.

Since the both stator and rotor arcs are chosen to be same angular length, (30^0 in mechanical angle), the air gap reluctance seen by the magnet, which contributes the most reluctance, is invariant with rotor position. Therefore, assuming that the PM flux linkage varies linearly at no load, as shown in Fig. 2, the voltage induced in the stator windings is rectangular due to Faraday's law. The polarity of this no-load voltage can be found by Lenz's law. Armature reaction causes the total flux to circulate through the companion-overlapped pair as can also be seen in the finite element flux contour plots in the forthcoming sections.

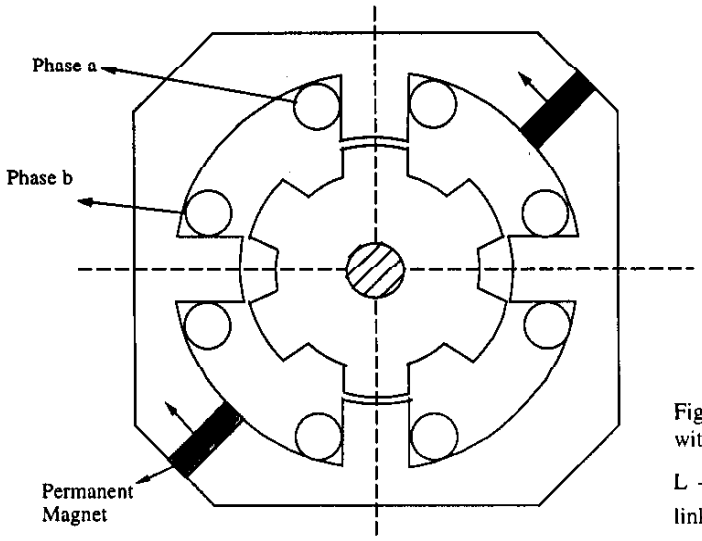

Fig. 1 A typical lamination for 4/6 DSPM Generator

The inductance profile of the stator windings can be deduced by examining the cross section of the machine shown in Fig. 1. As a rotor pole starts to overlap with a stator pole, i.e. full-misalignment, the adjacent rotor pole is totally under the stator pole of the other phase. In this position, the reluctance is a maximum. Considering that inductance is inversely proportional to reluctance, the phase inductance is minimum at this position. As the rotor rotates, reluctance seen by the stator winding becomes smaller, until the half-overlapped position between the rotor and stator poles is passed. At a half-overlapped position, the reluctance seen by the stator winding is a minimum, and hence the inductance is a maximum. After the half-aligned position, the reluctance starts to increase. When full-alignment is reached, the inductance becomes minimum again. Consequently, the active stator phase winding has a minimum inductance for a given active stator phase winding which occurs at both *aligned* and *unaligned* rotor positions. The maximum inductance occurs when the poles are *half-overlapped* as shown in Fig. 2.

The above analysis of the DSPM generator and the waveforms shown in Fig. 2 are based on first order approximations. However, in reality the machine inductance and back emf voltages are functions of current and rotor position.

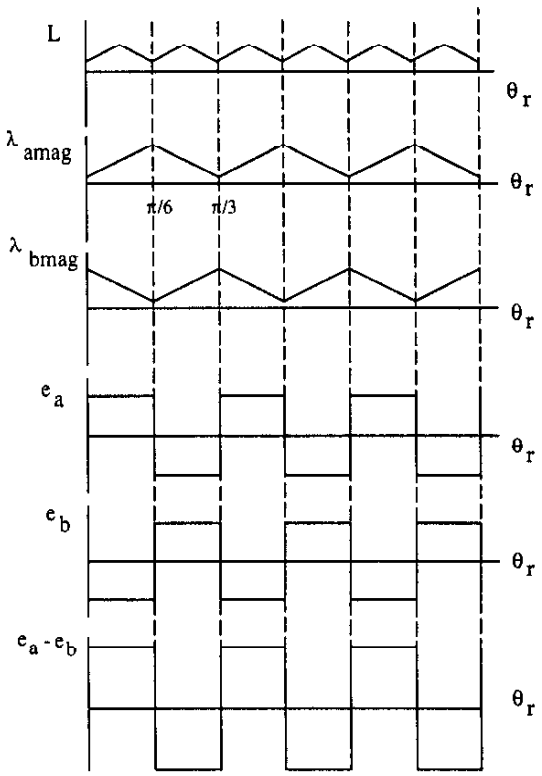

Fig. 2 The phase inductance and permanent magnet flux variations with respect to rotor position. From top to bottom:

L - inductance of phases a and b, λ_{amag}, λ_{bmag} - magnet flux linking a and b phases, E_a, E_b - emfs induced in a and b windings, e_a-e_b –emf if windings are connected in series.

3. FINITE ELEMENT ANALYSIS OF DSPM GENERATOR

To get a more accurate model of the DSPM generator, one may use flux-linkage versus current diagrams as has already been successfully utilized in the analysis of the variable reluctance machine's performance [2], [8]. This diagram is obtained by plotting the variation of the instantaneous phase current with respect to the instantaneous phase flux linkage. The data can either be collected by measuring real quantities via an experiment, or by using a numerical method such as finite element method analysis. The later approach is advantageous in terms of cost and time since it can be used to verify and improve the electromagnetic design of these machines before construction begins. From either means, much useful information can be obtained. For example, the power producing capability of the machine can be calculated and is equal to the area enclosed by the flux linkage vs. current trajectory multiplied by the number of the closed trajectories per revolution of the rotor.

A. FEM Modeling

In order to better include the external leakage effect of the permanent magnet of the DSPM generator, a circular or rectangular zero magnetic vector potential boundary is used which encircles the stator in the DSPM generator model. The size of the circular or

rectangular boundary condition is maintained sufficiently large such that neither the required time for the FEM computation and storage will be out of tolerable limits, nor the solution accuracy is compromised in the calculation of external leakage of the permanent magnets. Stator and rotor laminations are modeled as M-19 grade steel. Exact dimensions of the permanent magnets used in the prototype are used in the model. Also, the electromagnetic properties of 34 K Neodymium Iron Boron permanent magnet are obtained from the vendor and entered into the FEM database as tabulated in Table 1. Therefore, the modeling of the DSPM generator for finite element analysis is kept as close as possible to the geometry and electromagnetic properties of the actual prototype machine.

TABLE 1: Design #2 Magnetic Characteristic used in FEM for 34 K Neodymium Iron Boron Magnet

Magnetic Properties	Symbols	Units	Value
Relative Permeability	μ_r	-	1.04344
Magnetic Coercivity	Hc	A/m	-915,170
Magnetic Retentivity	Br	T	1.2
Magnetization	Mp	A/m	954,929

B. DSPM Windings and Excitation

For each pole of the DSPM generator, there are 6 turns of copper magnet wire. Each winding in the model can be considered as having two slots with positive and negative current in the model. For the FEM model of the DSPM generator, the windings are assumed to be connected in series, with one phase supporting the flux due to the permanent magnet, while the other phase opposes the flux due to the permanent magnet fulfilling Lenz's Law. This sequence depends on the position of rotor with respect to the stator (i.e., entering or leaving). The directions of the permanent magnet flux and armature reaction flux due to the current in the stator winding used in the FEM analysis are shown graphically in Fig. 3. It should be noted that a sink convention is used for the directions of the current and voltage.

C. FEM Results

The FEM analysis was carried out for different rotor angles ranging from full-alignment to full-misalignment for the DSPM generator. The full-alignment of the rotor is assumed to occur at 0 degrees while the full-misalignment occurs at 30 degrees (when the rotor tooth leaves the stator tooth) or -30 degrees (when the rotor tooth comes into alignment with the stator tooth). Note that for the DSPM generator the FEM solution of one pole flux, for the case where the rotor leaves the stator, will be the same as for the solution of the adjacent pole for the case where the rotor approaches the stator. Fig. 4 shows the flux plot of the DSPM generator for the 15-degree rotor position under a loaded condition.

Even though contour plots of the field variable magnetic vector potential A are extremely useful in analyzing and visualizing the magnetic field inside a machine, and the flux density distribution gives details on the degree of magnetic saturation, fringing, and demagnetization, useful information can also be extracted to assist lumped parameter analysis. Therefore, detailed studies of the magnetic flux linkage of the DSPM generator as a function of rotor position and current in the windings have been carried out using the finite element method, and the discrete results are shown in circles in Fig. 5. In Fig. 6, a different representation of the same data in Fig. 5 is given by changing the parameter to phase current.

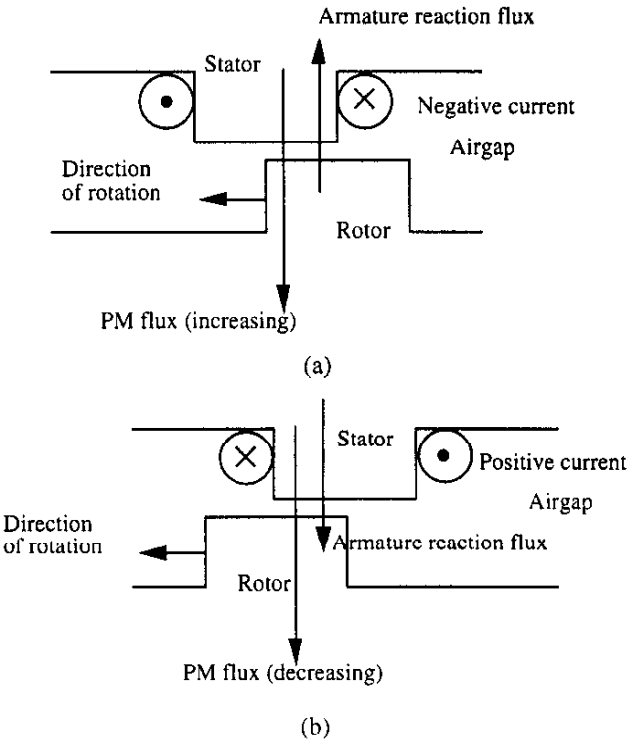

Fig. 3 Flux directions for DSPM generator; a-When rotor reaches stator, phase current is negative; b-When rotor leaves stator, phase current is positive.

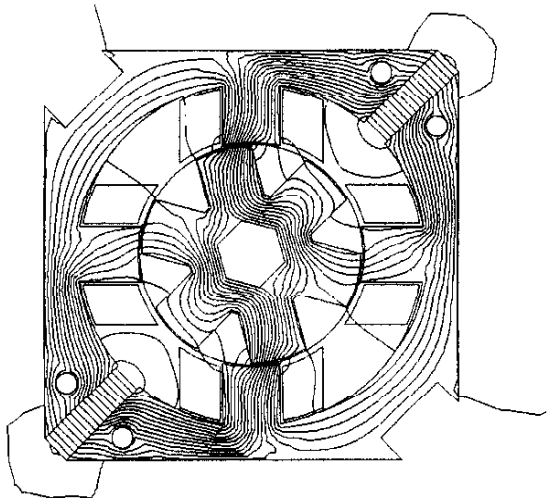

Fig. 4 Flux plot for 120 A condition at full-aligned rotor position for DSPM generator.

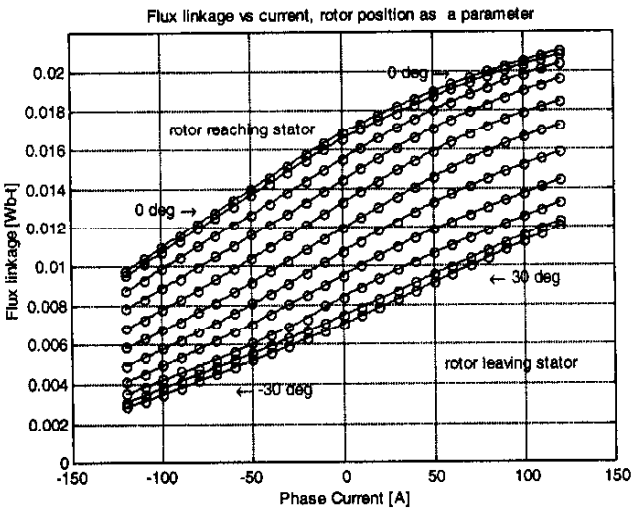

Fig. 5 FEM results showing flux linkage vs. current and rotor position is a parameter for a pole winding.

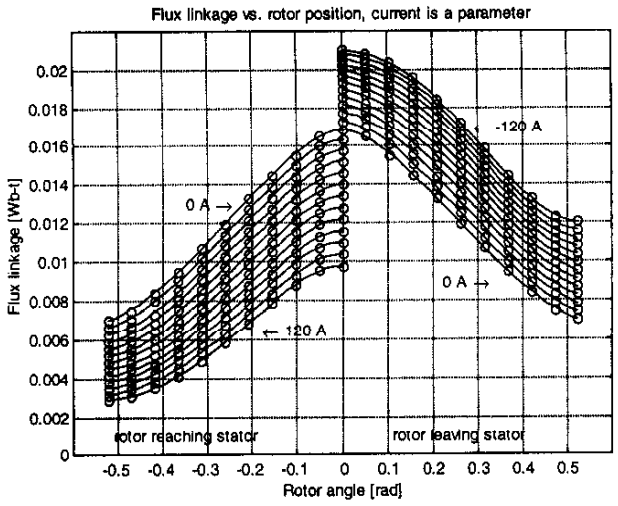

Fig. 6 Flux linkage vs. rotor angle for a pole winding for various current levels.

4. CUBIC SPLINE THEORY AND ITS APPLICATION TO DOUBLY-SALIENT MACHINES

The above analysis of the DSPM generator and its waveforms shown in Fig. 2 are based on the first order approximations. However, in reality the flux linked by the winding, inductance, and back emf voltages is a function of both rotor angle and current. Hence, a better design would be achieved if the machine were analyzed with more accurate modeling.

Even though looking at Fig. 5 is insightful in terms of observing saturation and the energy conversion loop, from the dynamic simulation perspective it is necessary to take the partial derivatives of flux linkage. In this case, one needs two partial derivatives, one of flux linkage with respect to rotor position and the other with respect to current.

To achieve this goal, cubic splines can be used in which cubic polynomials are utilized to connect data points where the resulting spline function has two continuous derivatives everywhere [12], [13]. Moreover, every individual cubic function is then connected at each data point (also called knot) forming a smooth curve. For a particular rotor position, if there are n points of data for a flux linkage λ, then the spline function $\lambda(i)$ will have n-1 cubic polynomials:

$$\lambda_k(i) = a_k (i - i_k)^3 + b_k (i - i_k)^2 + c_k (i - i_k) + d_k \quad (1)$$

where i is the instantaneous phase current at the interval of $i_k < i < i_{k+1}$ and subscript k is k = 1,2, ..., n-1. Fig. 7 depicts the application of spline theory to a λ versus i data set curve.

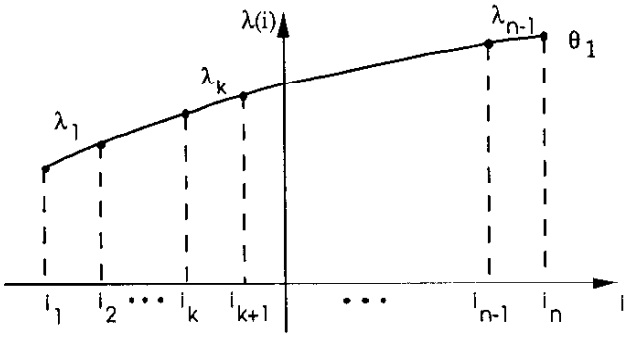

Fig. 7 Illustration of spline theory for flux linkage vs. current for a specific rotor position

Four parameters a_k, b_k, c_k, and d_k need to be determined for every segment. This can be done by evaluating four conditions for each segment. The first two conditions dictate that the polynomial end points of a particular segment must have the same value as the data points at either end. That is

$$\lambda_k (i_k) = d_k \quad (2)$$

$$\lambda_k (i_{k+1}) = a_k (i_{k+1} - i_k)^3 + b_k (i_{k+1} - i_k)^2 + c_k (i_{k+1} - i_k) + d_k \quad (3)$$

The other two conditions are related to the "smoothness" of the polynomials at their end points. Therefore, first and second derivatives of the polynomials must have smooth transitions at the data points.

$$\frac{d\,\lambda_{k+1}(i_{k+1})}{di} = \frac{d\,\lambda_k(i_{k+1})}{di} \quad (4)$$

$$\frac{d\,\lambda^2_{k+1}(i_{k+1})}{di^2} = \frac{d\,\lambda^2_k(i_{k+1})}{di^2} \quad (5)$$

A boundary condition is also needed for the solution. Mathematical algorithms are available to find the four unknown parameters for each segment and can be implemented in computer code. In the study being reported, the MATLAB spline toolbox was used.

5. PROCEDURE FOR NONLINEAR MODELING AND SIMULATION

The procedure to obtain the non-linear characteristic of the DSPM generator is as follows.

- Flux linkage vs. current curves for different positions of the rotor are obtained from the FEM analysis. The approach

includes important effects associated with conventional design such as the magnetic non-linearity of the iron parts (saturation effect), fringing at the non-overlapping stator and rotor pole tips, uneven distribution of the flux density, and the inner and outer leakage flux of the permanent magnets. As long as the accuracy of the FEM analysis is reasonable, the data obtained can be assumed accurate. The same analysis is valid if data are obtained through experimental measurement of flux linkage. The emf induced in the winding can be found by taking the derivative of the flux linking that coil with respect to time. Since the flux linking the coil is a function of the rotor position and current, one has to take partial derivatives. Mathematically, for a given phase

$$e = \frac{d\lambda}{dt} = \frac{\partial\lambda(\theta,i)}{\partial\theta}\frac{d\theta}{dt} + \frac{\partial\lambda(\theta,i)}{\partial i}\frac{di}{dt} \qquad (6)$$

$$e = BEMF(\theta,i)\frac{d\theta}{dt} + L(\theta,i)\frac{di}{dt} \qquad (7)$$

where the voltage e is the armature induced emf, λ is the total flux linking the winding, θ is the rotor position. The position and current dependent back emf and inductance terms are, respectively:

$$BEMF(\theta,i) = \frac{\partial\lambda(\theta,i)}{\partial\theta} \qquad (8)$$

$$L(\theta,i) = \frac{\partial\lambda(\theta,i)}{\partial i} \qquad (9)$$

- To evaluate these partial derivatives, the data points obtained from finite element analysis must have well behaved derivatives, i.e. a smooth function otherwise, the differentiation will not be accurate. The spline method is used to connect the flux linkage data points for different rotor positions. Therefore, the curves are smooth and can be evaluated for partial derivatives. The smooth curves of flux linkage vs. current for different rotor positions are obtained by the spline method as shown in Fig. 5. One can observe the saturation occurring when the rotor pole begins to leave the excited stator. Similarly, when the rotor pole approaches the stator, pole armature reaction occurs and reduces the flux in the airgap. Fig. 5 can be mapped into a flux linkage vs. rotor angle curves with current as a parameter as shown in Fig. 6. Armature reaction can be readily seen either when the rotor leaves or reaches the stator as the machine is loaded.

- Results for the partial derivatives $\frac{\partial\lambda(\theta,i)}{\partial\theta}$ and $\frac{\partial\lambda(\theta,i)}{\partial i}$ of a winding are obtained by taking the derivative of spline functions developed and are shown in Fig. 8 and Fig. 9. In Fig. 8, one can observe that the armature reaction effect plays an important role for the magnitude of the back emf. As the machine is loaded, the back emf reduces in magnitude when the rotor reaches the stator. When the rotor is leaving the stator, the magnitude and shape of the generated voltage are distorted due to the armature reaction. From Fig. 9, it is seen that the active inductance term has a discontinuity at the aligned position since the armature reaction flux changes direction. The results obtained from conventional magnetic circuit analysis are L_{min}=22 μH and L_{max}=26.1 μH per pole winding. Therefore, it can be seen that the minimum inductance obtained from the nonlinear analysis is one and one-half times larger than that from conventional magnetic circuit analysis while the maximum inductance at lower current reaches twice that from conventional analysis. Also, active inductance decreases as the machine is loaded. This phenomenon is more drastic when the rotor is leaving the stator. Both Fig. 8 and Fig. 9 enable the analyst to visualize what is happening to instantaneous generated voltage and inductance as the phase current and rotor position are changed. At this point it should be mentioned that oscillatory behavior of the derivative may occur due to the nature of the differentiation operation if the data points are slightly rounded from finite element analysis. To prevent the problem of oscillation, another interpolation of the obtained partial derivatives should be made based on the square of the error.

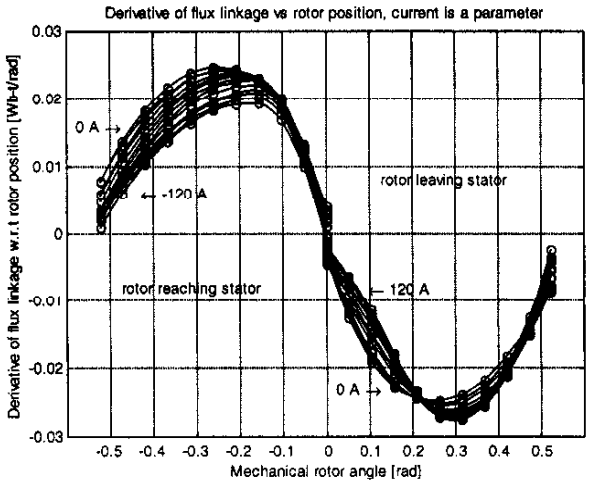

Fig. 8 The partial derivative of pole flux linkage with respect to rotor position, i.e. $\frac{\partial\lambda(\theta,i)}{\partial\theta}$ (current is a parameter).

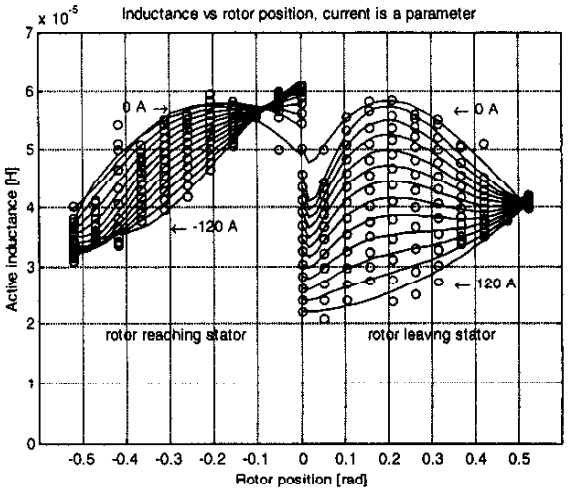

Fig. 9 The partial derivative of pole flux linkage with respect to phase current, i.e. $\frac{\partial\lambda(\theta,i)}{\partial i}$ for incremental rotor positions.

6. EXPERIMENTAL STATIC TESTING OF THE DSPM GENERATOR

Using the analysis methods described a prototype DSPM generator has been designed, built and tested to evaluate its performance. The purpose of the static testing of the prototype generator is to obtain the flux linkage with respect to the current value or the instantaneous inductance with rotor position as a parameter. This information can be thought of as a *performance signature* of the machine. From this data, many important parameters can be extracted to verify whether the design calculations, especially finite element analysis results, are in good correlation with the prototype.

For static testing purpose, a bar fixed to the shaft is made to position the rotor. A C-clamp is used to prevent the bar from moving and to hold the rotor at any desired angular rotor position. One variac and two transformers are cascaded to give precision control of the low input voltage to obtain the necessary rated current level of 80 A. A sinusoidal voltage is applied to the machine where the two phase windings are connected in series. For each rotor position, the sinusoidal voltage is increased until 120 A peak current is achieved. Fig. 10 shows the voltage and current waveform for the full-unaligned position.

Current and voltage waveforms across one phase are sensed and stored in a disk from an oscilloscope. Data recorded is transferred to a computer where numerical integration is done to obtain the flux linkage for different rotor positions. The numerical integration that is used can be obtained directly from the Faraday's law of induction:

$$e(t) = \frac{d\lambda}{dt} = v(t) - R\, i(t) \qquad (10)$$

Flux linkage can be obtained as

$$\lambda = \int_0^t (v - R\, i)\, dt + \lambda_{0r} \qquad (11)$$

where v is the instantaneous voltage across the phase, R is the phase resistance, i is the instantaneous phase current, and λ_0 is the initial value of the flux linkage.

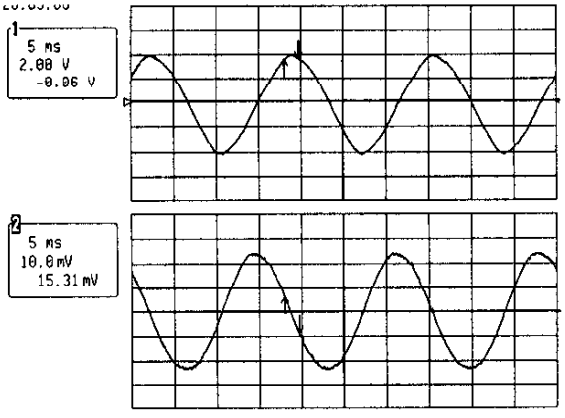

Fig. 10 Static test results for the full-unaligned position:

Top trace: Phase Voltage 2 V/div Bottom trace: Phase current 50 A/div

A. Comparison of Static Experiment Results With FEM Results

Estimation of the inductance plays a crucial role in doubly salient topologies due to the importance of current commutation in power production capability. The inductance of a DSPM machine is a function of both current and rotor position. Considering the fact that the slope of the flux linkage vs. current curve is the instantaneous inductance, it is possible to compare the results obtained from experiment with those from FEM analysis.

Fig. 11 shows the results for the flux linkage versus current for three important rotor positions by making the assumption that the prototype generator has the same permanent magnet flux linkage as that of the finite element analysis. Since the slope of these curves at any instant is the incremental inductance of the generator, the inductance values obtained from the testing are in good correlation with those obtained from the finite element analysis. These overlaid plots convincingly suggest that the nonlinearity of the DSPM machine can be predicted by using tools such as nonlinear finite element analysis. From the curves, it can be observed that the steel laminations used in the prototype machine saturate at a higher flux density than that of the steel characteristic used in the finite element analysis. Another source of error is the fact that end turn leakage, which is not included in the finite element analysis. This leakage component introduces an extra inductance that is independent of rotor position.

7. NO-LOAD ROTATIONAL TESTING

This test aims to obtain the flux linkage with respect to position or back emf voltage. A separately-excited dc motor is used as a prime mover to run the DSPM generator at various speeds. Individual voltages of the two phases and the sum of the voltages of the two phases are measured. Fig. 12 shows the waveforms obtained at 3000 rpm.

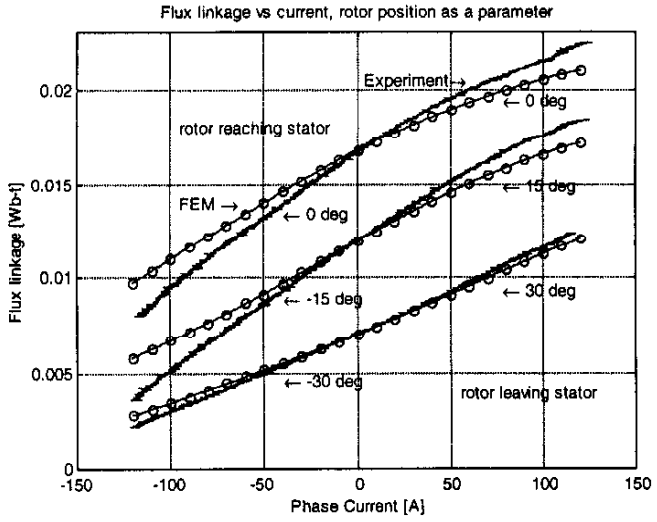

Fig. 11 Flux Linkage vs. Current for aligned (0 deg), half-aligned (15 deg), and full-misaligned (30 deg) positions. Straight curves are from experimental results: circled data points are from finite elements.

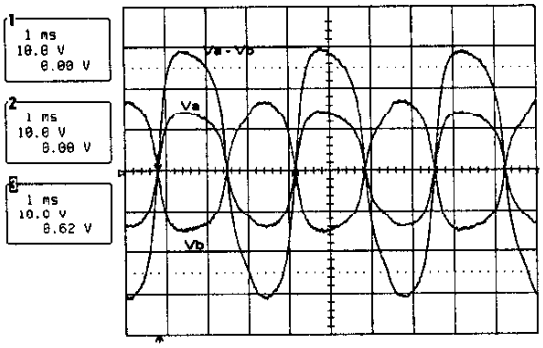

Fig. 12 Phase voltages (V_a and V_b) and sum of the two phase voltages (V_a-V_b) at 3000 rpm. (All plots are 10V/div)

TABLE 2 Magnitude of output voltage at various frequencies.

Frequency (Hz)	Magnitude (V)
300	33
600	2.75
900	4.82
1500	1.37

As can be seen from the waveforms, individual phase voltages are not exactly rectangular. This is expected, since flux linking the windings does not change exactly in a triangular fashion due to the fringing (especially at non-overlaping poles) and saturation in the generator.

To analyze the frequency content of the output voltage, a Fast Fourier Transform (FFT) of the total output voltage is performed. Fig. 13 shows the magnitude of various frequency components of the output voltage. Table 2 documents the magnitude of voltages for significant frequency components.

A. Comparison of No-Load Experiment Results with FEM Results

To assess the accuracy of our finite element modeling and cubic spline modeling with respect to actual machine performance, the back emf voltages obtained from FEM analysis and experimental data are overlaid as shown in Fig. 14. It is observed that experimental data is in good correlation with the predicted results.

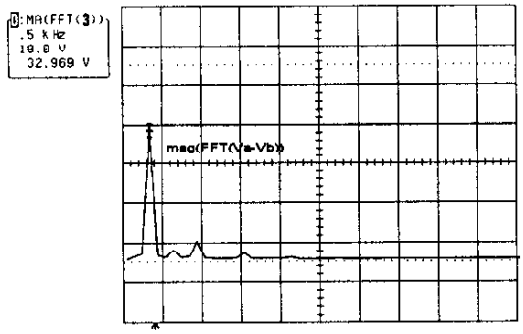

Fig. 13 Magnitude of FFT of the total voltage with respect to frequency. (Voltage 10V/div, frequency 500 Hz/div)

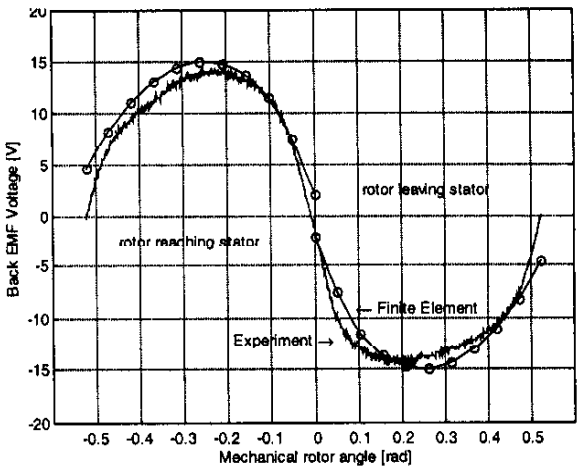

Fig. 14 Comparison of Experimental results vs. FEM: No-load back emf of one phase at 3000 rpm.

8. EXPERIMENTAL RESULTS AND NONLINEAR SIMULATION

The ac voltage output of the DSPM generator can easily be rectified to obtain a dc voltage. As a case study, a bridge rectifier is used for this purpose, assuming that the dc link current is essentially constant due to a large dc link inductor as shown in Fig. 15. Waveforms obtained from the experiment are shown in Fig. 16. The generator is run at 2270 rpm and the dc link current loading is 41.2 A.

A. Comparison of Experiment Results with Nonlinear Simulation

A simulation is also done using the nonlinear results obtained to verify the accuracy of the modeling. By using the sink convention ($i = -i_{ac}$), the stator current is

$$\frac{di}{dt} = \frac{\pm V_{dc} - (R_a + R_b)\, i - (BEMF_a(\theta,i) + BEMF_b(\theta,i))\,\frac{d\theta}{dt}}{L_a(\theta,i) + L_b(\theta,i)} \qquad (12)$$

where results for partial derivatives $BEMF_x(\theta,i)$ and $L_x(\theta,i)$ for each phase are found by iteration from the look-up table stored in the simulation. Diode voltage drops (2.5 V) are also included in the simulation. Stator current is obtained by simulating eqn.12 and results are shown in Fig. 17. In this simulation, the dc link current and rotor speed are set to same as those of the experiment.

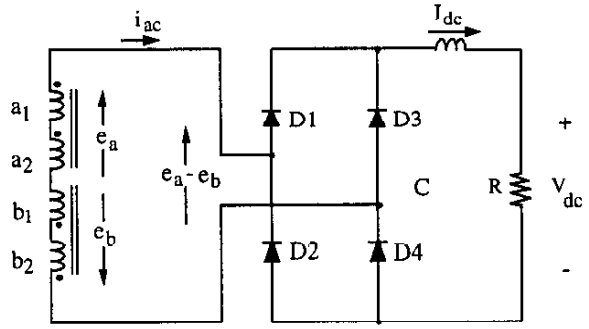

Fig. 15 Rectification with constant dc current.

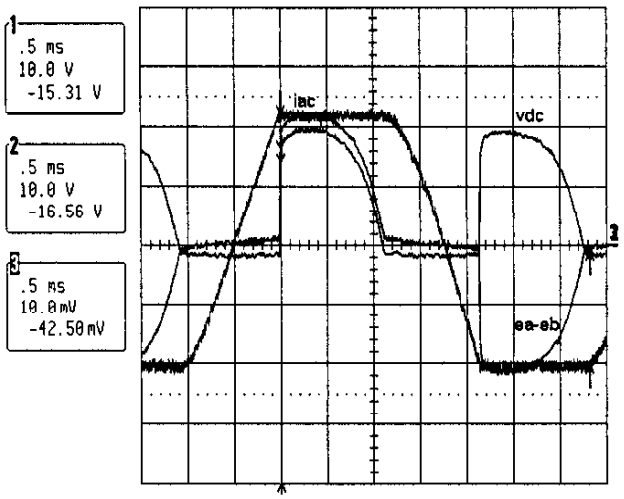

Fig. 16 Experimental results: (Traces: Voltages 10 V/div, current 20 A/div)

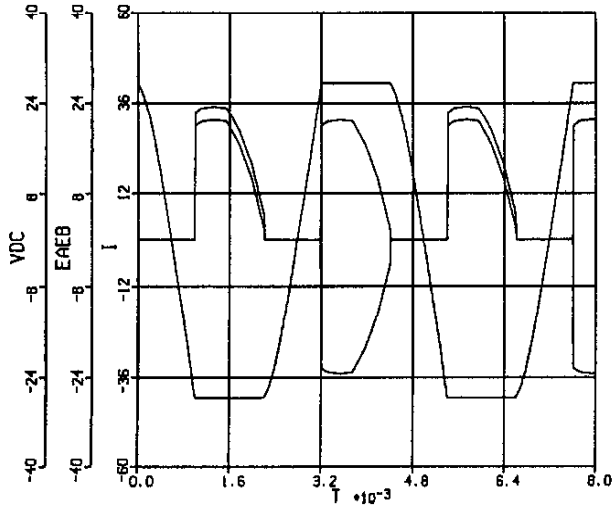

Fig. 17 Simulation results: Rectified voltage, voltage e_a-e_b and current i ($i = -i_{ac}$).

DC output power is calculated as 379 W experimental, while it is 368 W from the simulation. Also, the commutation times of current from the experiment and lab data are 105μs and 100μs, respectively. Therefore, a good correlation is also achieved in this portion of the waveform.

Fig. 18 illustrates other important quantities for the same simulation. It can be noted that waveforms of the inductance and the back emf of the machine are much different than using the first approximation shown in Fig. 2. For example, the inductance values obtained from the conventional analysis are one and half to two times less than those obtained from nonlinear analysis. Therefore, the prediction of overall performance calculation can be done more realistically by using nonlinear modeling, since both inductance and back emf terms determine the commutation period, and hence power transfer from the ac generator output to the dc load.

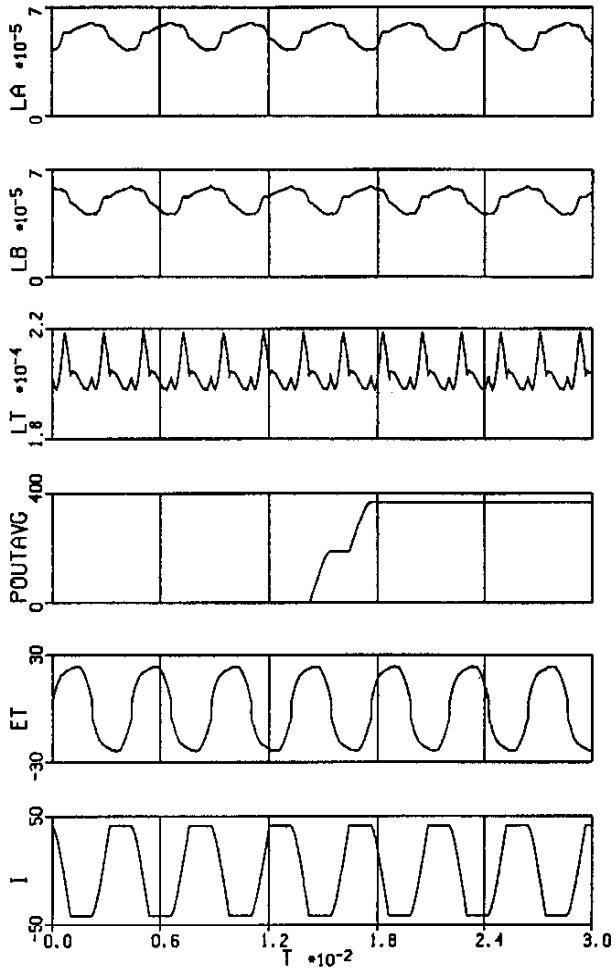

Fig. 18 Nonlinear simulation results: (Top to bottom: Phase a and b inductance, total inductance L_t, average dc output power P_{outavg}, back emf voltage (BEMF) E_t, and current I.)

9. CONCLUSION

In this paper, it is demonstrated that cubic splines can be gainfully used to take the partial derivatives of flux linkage obtained from the finite element analysis or measurement. A better visualization of the instantaneous inductance and back emf terms can be made, and also used to check design goals. This approach also enables the analyst to readily simulate the machine and power electronics circuitry together. The accuracy of the proposed approach has been compared with experimental results and a good correlation is achieved. It has been also shown that permeance analysis underestimates the inductances by one and one-half to two times with respect to nonlinear analysis compared to those obtained from nonlinear analysis.

Cubic spline algorithms are readily available in the literature or in software packages. The procedure given in this paper can also be used for any highly-nonlinear machine for which generalized machine theory and lumped-parameter modeling either do not exist or fail to give accurate results.

10. ACKNOWLEDGEMENT

Wisconsin Electrical Machine and Power Electronics Consortium (WEMPEC) at University of Wisconsin-Madison is gratefully acknowledged for funding this project. Thanks is also given to Miller Electric Company for construction of the generator.

REFERENCES

[1] Sarlioglu, B., Zhao, Y., Lipo, T.A., "A Novel Doubly Salient Single Phase Permanent Generator". *IEEE IAS Annual Meeting*, Denver, CO, Oct. 2-6, 1994, pp. 9-15.

[2] Sarlioglu, B., Lipo, T.A., "Comparison of Power Production Capability Between Doubly Salient Permanent Magnet and Variable Reluctance Type Generators", 1995 Aegean Conference on Electrical Machines and Power Electronics, Kusadasi, Turkey, June, 1995.

[3] Lipo, T.A., Li, Y., Luo, X., Sarlioglu, B., "Doubly Salient Permanent Magnet Machines- A Progress Report", International Symposium on Electric Power Engineering, Stockholm, June 18-22, 1995.

[4] Liao, Y., Liang, F., and Lipo, T.A., "A Novel Permanent Magnet Motor with Doubly Salient Structure", *IEEE IAS Annual Meeting*, Houston TX, Oct. 5-8, 1992, pp. 308-314.

[5] Shakal, A., Liao, Y., Lipo, T.A., " A New Permanent Magnet Motor Structure with True Field Weakening", IEEE International Symposium on Industrial Electronics, Budapest, Hungary, June 1993, pp. 19-24.

[6] Liao, Y. and Lipo, T.A., "Sizing and Optimal Design of Doubly Salient Permanent Magnet Motors", IEE 6th International Conference on Electrical Machines and Drives, Sept. 8-10, 1993, pp. 452-456.

[7] Miller, T. J. E., and McGlip, M., "Nonlinear Theory of Switched Reluctance Motor for Rapid Computer-Aided Design", IEE Proceedings, Vol 137, Pt. B, No.6, November, 1990.

[8] Moallem, M.and Ong, C.M., "Predicting the Torque of a Switched Reluctance Machine From its Finite Element Solution", *IEEE Transactions Energy Conversion*, Vol.5, No.4, December 1990.

[9] Miller, T.J.E, "Converter Volt-Ampere Requirements of the Switched reluctance Motor Drive", IEEE-IAS Annual Meeting, Chicago, IL, October, 1984.

[10] Ray, W.F., Lawrenson, P. J., Davis, R.M, Stephenson, J.M., Fulton, N.N., and Blake, R.J., "High-Performance Switched Reluctance Brushless Drives", IEEE-Transactions on Industry Applications, Vol. IA-22, No.4, July/August 1986.

[11] Stephenson, J.M. and Corda, J., "Computation of Torque and Current in Doubly Salient Reluctance Motors from Non-linear Magnetisation data", Proc. Inst. Elec. Eng., vol. 126, pp. 393-396, May 1979.

[12] Borse, G.J, Numerical methods with MATLAB : *A Resource for Scientists and Engineers*, PWS Publishing, 1997.

[13] Burden, L.B. and Faires, J.D., *Numerical Analysis*, PWS Publishing company, 1993.

APPENDIX

Two pictures are shown in Fig. A.1 and Fig. A.2 illustrating the assembly and experimental setup.

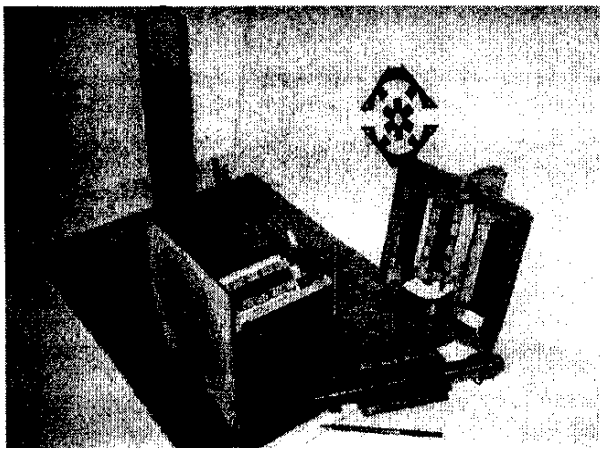

Fig. A.1 The DSPM generator before assembly. This setup is used for static measurement. A level is used to keep the rotor position constant.

Fig. A.2 The experimental setup for DSPM generator. DSPM generator is on left and seperately excited dc machine is on right.